Release of gold-bearing fluids in convergent margin magmas prompted by magnetite crystallization

Weidong Sun[1,2], Richard J. Arculus[3], Vadim S. Kamenetsky[1,4] & Raymond A. Binns[3,5]

[1]*Max-Planck-Institut für Chemie, Mainz, Postfach 3060, Mainz 55020, Germany*
[2]*Research School of Earth Sciences, Australian National University, Canberra, ACT 0200, Australia*
[3]*Department of Earth and Marine Sciences, Australian National University, Canberra, ACT 0200, Australia*
[4]*Centre for Ore Deposit Research and School of Earth Sciences, University of Tasmania, GPO Box 252-79, Hobart, Tasmania 7001, Australia*
[5]*CSIRO Exploration and Mining, North Ryde, NSW 1670, Australia*

A relationship between convergent margin magmas and copper–gold ore mineralization has long been recognized[1–6]. The nature of the genetic link is controversial, particularly whether the link is due to high-oxygen-fugacity (f_{O_2}) melts and fluids released from subducted slabs[5–7] or to brine exsolution during magmatic evolution[4]. For submarine, subduction-related volcanic glasses from the eastern Manus basin, Papua New Guinea, we here report abrupt decreases in gold and copper abundances, coupled with a switch in the behaviour of titanium and iron from concentration increases to decreases as SiO_2 rises. We propose that the abrupt depletion in gold and copper results from concurrent sulphur reduction as a result of f_{O_2} buffering, causing enhanced formation of copper–gold hydrosulphide complexes that become scavenged from crystallizing melts into cogenetic magmatic aqueous fluids. This process is particularly efficient in oxidized arc magmas with substantial sulphate. We infer that subsequent migration and cooling of exsolved aqueous fluids create links between copper–gold mineralization and arc magmatism in the Manus basin[8,9], and at convergent margins in general[1–6].

Most of the world's copper–gold (Cu–Au) ore deposits (for example, epithermal/porphyry types) are associated with convergent margin magmas[1–7], usually characterized by a high f_{O_2} (ref. 6). Although these ore metals might ultimately have been recycled from the subducted slab[6], the subarc mantle is not significantly enriched in Au and Cu (ref. 7), and so far the relationship between Cu–Au mineralization and subduction-derived magmas remains controversial. Many different genetic models have been developed to explain this relationship[4–7], building mainly on the fact that subduction zone magmas have a relatively high f_{O_2}. These models include the possibilities that slab-released oxidizing fluids are capable of concentrating metals in the sulphide-bearing metasomatic assemblages of the mantle wedge that become preferentially melted during formation of arc magma[7], and that high f_{O_2} might promote the oxidation of residual sulphide in the wedge, liberating chalcophile elements[3,6]. Other models favour sulphide undersaturation in the magmas[6], thus increasing magmatic enrichment in incompatible Au and Cu during crystallization.

The behaviour of Au in evolving magma systems is not well understood[10]. Early studies suggested that Au is compatible during magma formation[11] but this is not always true[12]. Gold concentrations in arc volcanic rocks, although variable, increase during the early stage of magmatic evolution (incompatible behaviour), then decrease in felsic rocks (apparently compatible)[10,13]. One possible explanation is that under special chemical and physical conditions, a considerable amount of Au can be dissolved in H_2O-rich vapour[14] and fluids[4,7,15] and therefore potentially become lost through degassing of H_2O-saturated arc magmas. The widely variable Au concentrations reported for subaerially erupted arc volcanic rocks[10] might partly reflect different degrees of Au loss during degassing. This process is less effective for eruptions on the deep sea floor. In this study we analysed submarine, subduction-related volcanic glasses and olivine-hosted glass inclusions (entrapped parental melts) from the eastern Manus basin (dredged in the depth range 1,640–2,000 m) using a laser-ablation, inductively coupled plasma-source mass spectrometry (LA-ICP-MS) technique refined for quantifying trace elements at concentrations less than 1 part per 10^9 (p.p.b.)[16–18]. These data provide an outstanding opportunity to understand the behaviour of Au and Cu during the fractionation of arc-type magmas.

Essentially aphyric eastern Manus basin glasses range in composition from basalt to rhyodacite, with SiO_2 contents from 50.4 to 74.1 wt%, and MgO contents from 11.7% to 0.3% (calculated anhydrous). They have strong arc geochemical affinities, with relative depletion in Nb and Ta and enrichment in H_2O, Cs, Rb, Ba, U and Pb (refs 18,19). Our sample set (Table 1) from a large CSIRO collection of well-characterized samples was selected as a coherent fractionation suite, evidently derived from closely comparable basaltic parents in adjacent volcanic edifices (Supplementary Figs 1 and 2). Notably, TiO_2 and FeO (total) change from

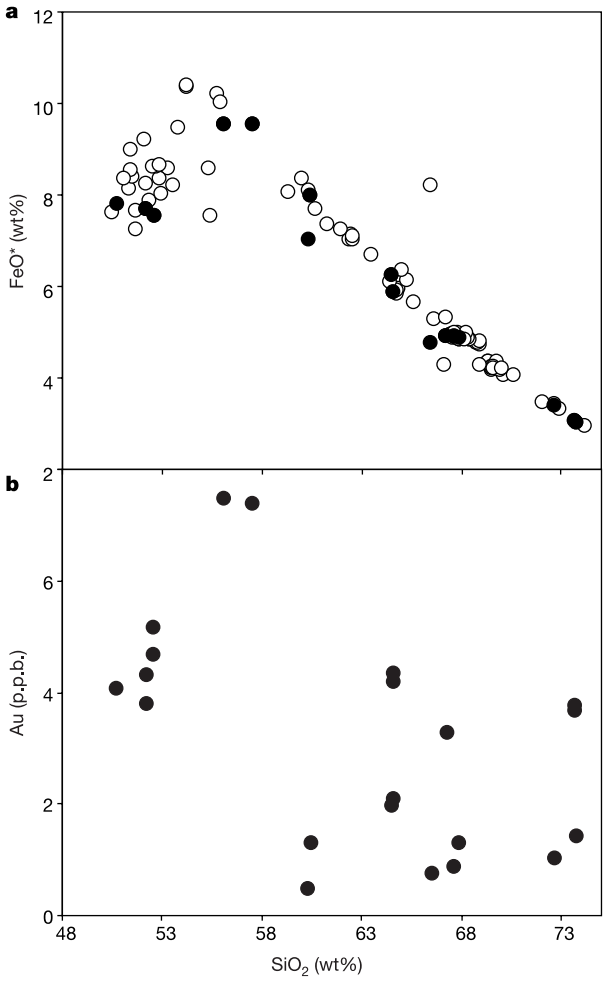

Figure 1 Selected compositional characteristics of eastern Manus basin volcanic glasses. **a**, SiO_2 wt% versus total Fe as FeO (FeO*); **b**, SiO_2 wt% versus Au. SiO_2 and FeO total are recalculated to 100% volatile-free with Fe^{3+}/Fe_{total} set at 0.25. Gold was determined with the same method as that used previously for analysing p.p.b. to sub-p.p.b. levels of Re (refs 16–18; see Supplementary Information for detail).

©2004 Nature Publishing Group

positive to negative correlations with SiO_2 at ~58% SiO_2 (Table 1, Fig. 1a, Supplementary Fig. 2), corresponding to a significant change in magma evolution arising from cessation of olivine crystallization and commencement of titanomagnetite crystallization. Gold concentrations in these highly vesicular Manus glasses mostly range from 0.9 to 7.8 p.p.b. (Table 1), comparable to previous data[13] but with better sensitivity and precision. Two glass pieces include points extremely enriched in Au (up to 73 p.p.b.; Table 1), similar to previous observations on Re distribution[18]. However, their ablation spectrum patterns show short-lived high-Au signals that are not directly coupled with Re (Supplementary Fig. 3), suggesting that these elements are in part hosted by different trace minerals (such as sulphides) possibly within vesicles or fluid inclusions. Gold in olivine-hosted melt inclusions is high and varied (3.2–8.7 p.p.b., Table 1), spanning its abundance in the host glass (4.1 p.p.b.). Cu distribution within specific glasses is more homogeneous.

The abundance of Cu measured by LA-ICP-MS in the eastern Manus basin samples initially increases with increasing SiO_2, reaching peak values at ~58% SiO_2. Significantly, Cu concentrations drop abruptly beyond 58% SiO_2 (Table 1, Supplementary Fig. 2). Conventional bulk Cu analyses of 96 aphyric glasses from the Manus basin exhibit an identical trend. Gold concentrations, excluding anomalies mentioned above, show a similar behaviour with a distinct but less marked decrease beyond 58% SiO_2 (Fig. 1b). Total S in the glasses displays a less coherent but similar pattern, with a more gradual decrease beyond peak values of ~350 p.p.m. at ~58–64% SiO_2. In contrast, mafic melt inclusions have considerably higher and varied total S up to 1,000 p.p.m. (Supplementary Fig. 4). These indicate that even the mafic glasses have lost S, probably in the form of sulphate[19,20], which did not remove much, if any, Au from the magma. The Yb/Au and Yb/Cu ratios of the more mafic glasses and their melt inclusions are fairly constant (Fig. 2), indicating that Au and Yb behave in a similarly incompatible manner during early fractional crystallization. The Yb/Au ratios of melt inclusions hosted in olivine ($Fo_{89–91}$) are comparable to those of the host basalt glass, precluding significant Au loss during initial fractional crystallization. The average Yb/Au (350) and Cu/Au (25,000) of mafic samples are close to but slightly lower than primitive mantle values (440 and 30,000 respectively)[21].

By contrast, the Yb/Au and Yb/Cu values of more felsic glasses (>58% SiO_2) are variable and considerably higher than those of the mafic glasses and melt inclusions, reflecting the abrupt decreases in Au and Cu concentrations (Table 1, Fig. 2) requiring a process of removal of Au and Cu at ~58% SiO_2 during magma evolution. Low Cu and Au in felsic magmas has previously been attributed to partitioning of these metals into magnetite[10,13], to pre-eruptive degassing[13] or to precipitation of magmatic sulphides[5]. Sulphide precipitation is an unlikely explanation for the eastern Manus suite given low total S contents in glasses (Supplementary Fig. 4) and given the absence or extreme rarity of sulphide globules in glasses or occasional cumulate xenoliths. Preliminary LA-ICP-MS analysis of titanomagnetite in an east Manus basin andesite (<6 p.p.b. Au, 2.9 p.p.m. Cu; see also ref. 10) indicates that extraction of this mineral will not account for the marked diminution of these metals in glasses at ~58% SiO_2. All of the magmas (mafic to felsic) from the eastern Manus basin are volatile-saturated, as shown by abundant fluid inclusions in olivine and fluid bubbles in glasses[19,22]. Consequently, sustained pre-eruptive degassing[23] does not on its own produce the marked change in behaviour of Au and Cu at ~58% SiO_2, coinciding with the onset of magnetite crystallization.

Gold and Cu are both highly chalcophile elements whose behaviour is controlled by the abundance and oxidation state of S, for example, as a HS-bearing complex in fluids[24]. They can also partition into Cl-rich aqueous fluids, as a Cl-bearing complex[25]. Given the high abundance of Cl in arc magmas, a Cl complex might

Table 1 **Selected major and trace element compositions of Manus glasses and melt inclusions**

Sample no.	*n*†	SiO_2† (wt%)	TiO_2 (wt%)	FeO* (wt%)	Cu† (p.p.m.)	1σ	Yb† (p.p.m.)	1σ	S (p.p.m.)	Au (p.p.b.)	1σ
MD6	3	73.68	0.36	3.06	17.4	0.4	4.73	0.09	0	1.47	0.11
MD39	3	72.55	0.39	3.46	19.4	0.2	4.31	0.03	67	1.06	0.17
87DR-I	1	73.53	0.43	3.12	16.0	0.2	4.25	0.06	70	3.70	0.20
87DR-II	1	73.53	0.43	3.12	17.7	1.0	4.46	0.02		73.5	18.2
87DR-III	1	73.53	0.43	3.12	18.3	0.7	4.40	0.02		3.81	0.19
MD28	3	67.76	0.67	4.91	19.6	0.1	3.89	0.09	37	1.35	0.06
MD65	3	67.53	0.67	4.95	18.9	0.1	3.39	0.05	23	0.92	0.15
MD114	3	67.14	0.75	4.97	28.1	0.3	3.58	0.01	77	3.31	0.19
MD28B†	5	66.38	0.82	4.80	20.1	1.2	3.6	0.1		0.79	0.56
MD36	3	64.40	0.86	6.29	25.6	2.3	4.0	0.7	85	2.02	0.61
MD53A-I	1	64.49	0.83	5.94	30.7	0.2	3.32	0.06	93	4.22	0.54
MD53A-II	1	64.49	0.83	5.94	32.2	0.1	3.47	0.03		4.37	0.54
MD53A-III	1	64.49	0.83	5.94	28.2	0.2	3.52	0.02		2.13	0.18
MD36B†	5	60.19	0.97	7.09	35.2	7.9	3.2	0.3		0.51	0.05
MD53B	3	60.35	1.01	8.05	34.6	0.9	3.4	0.1	190	1.33	0.16
MD7	2	57.42	1.05	9.60	234	1.3	2.73	0.02	150	7.42	0.6
86DR	3	56.01	0.75	9.58	197	2.8	2.38	0.05	93	7.51	0.24
MD101A	3	52.47	0.40	7.59	108	0.5	1.41	0.05	20	4.73	0.75
MD101B	3	52.47	0.40	7.59	117	1.6	1.67	0.06	67	5.20	0.79
MD3-I	1	52.08	0.41	7.75	100.7	0.5	1.29	0.01	47	3.84	0.21
MD3-II	1	52.08	0.41	7.75	102.6	0.3	1.37	0.01		4.34	0.21
MD3-III	1	52.08	0.41	7.75	104.1	0.6	1.39	0.02		31.3	9.9
MD38†	5	50.60	0.42	7.87	108	3	1.12	0.01	108	4.10	0.20
Melt inclusions in olivine (MD-38)§											
M5D					191	4	1.74	0.016		6.2	0.2
M5D′					223	22	1.68	0.018		4.7	0.3
M6D					267	42	2.45	0.028		7.2	0.6
M6D′					173	9	2.45	0.02		8.7	0.9
M7C					180	3	1.86	0.023		4.3	0.2
M7C′					159	9	1.67	0.019		3.9	0.2
M11C					114	3	1.06	0.014		3.2	0.2
M12B					112	2	1.04	0.014		3.3	0.2

Major elements were analysed by X-ray fluorescence recalculated to 100% volatile-free with Fe^{3+}/Fe_{total} set at 0.25. The major elements of melt inclusions have not been analysed; an estimated 12 wt% CaO was adopted for LA-ICP-MS data reduction[19], which might introduce offsets but has no effects on ratios[17]. *n*, number of analyses. Trace elements are averages when $n \geq 2$. FeO*, total Fe as FeO.
† Data from ref. 18.
‡ Major elements from ref. 19.
§ Heterogeneous samples; each row represents one analysis on an individual piece of glass.

©2004 Nature Publishing Group

be important in scavenging Au and Cu out of the magmas but there are no experiments so far to demonstrate which complex is more important at magmatic temperature and pressures. Experiments at 100 MPa, in a high-chloride (total Cl = 2 molal) and low-H_2S system show that with increasing temperature $AuCl_2^-$ becomes the dominant species[25]. In contrast, experiments at 50 MPa show that with increasing temperature the solubility of Au increases as a HS complex[24,26]. In crustal magma chambers at low pressures, a HS complex is therefore likely to be the main species during early stages of magma evolution. This hypothesis is supported by other observations. The high CO_2 concentrations[19,20,22] and f_{O_2} characteristic of Au deposits in the eastern Manus basin magmas indicate that Au^+ is the favoured ionic state[27]. As one of the softest cations, Au^+ forms stronger complexes with soft ligands (such as HS^-) than with moderately hard anions such as Cl^- (ref. 27). Consequently, we propose Au and Cu abundances in the Manus basin melts and associated fluids to be largely governed by reduced S complexes.

The cogenetic Manus basin melts from basalt to rhyodacite have a relatively constant Fe^{3+}/Fe total of ~23 atom% (Supplementary Fig. 5). This implies an f_{O_2} uniformly about $2\log_{10}$ orders more oxidized than the synthetic fayalite–magnetite–quartz buffer[28], which is typical for igneous rocks associated with Au ore deposits[6]. A change in magmatic Ti and Fe compositional trends in the Manus basin suite (Fig. 1a, Supplementary Fig. 2) controlled primarily by the commencement of titanomagnetite ($Fe^{2+}Fe_2^{3+}O_4$–$Fe_2^{2+}TiO_4$ solid solution) crystallization should be accompanied by changes in relative Fe redox ratio in the absence of f_{O_2} buffering. We propose that the constant relative redox state over the compositional range of the Manus basin magmas is paralleled by sustained redox buffering and exchange between exsolved fluid and magma. Because of the high f_{O_2}, sulphate dominates in fluids associated with the mafic magmas, as confirmed by the presence of sulphate minerals in fluid bubbles within olivine-hosted melt inclusions[20,22,23]. However, the onset of magnetite fractional crystallization and increased rate of total Fe and particularly Fe^{3+} removal from the magma results in a shift in this redox exchange[29]:

$$8FeO + SO_4^{2-} = 4Fe_2O_3 + S^{2-}$$

Reduction of SO_4^{2-} to S^{2-} in the melt promotes the formation of Au and Cu hydrosulphide complexes, which efficiently partition into a coexisting high-temperature aqueous supercritical fluid[24,26], explaining the observed sharp depletion of Au and Cu in the felsic Manus glasses.

The escape of deep-seated Cu–Au rich magmatic fluids, derived thereby at the changeover from olivine to magnetite crystallization in the source chamber, provides the critical link between subduction-related magmas and Cu–Au ore deposits in modern and fossil arcs. Cooling at depth of upwardly mobilized fluids will create typical convergent margin porphyry/epithermal Cu–Au deposits. At upper crustal levels, ascending magmatic fluids may mix with seawater and with metals released during the hydrothermal alteration of a volcanic pile to form Cu–Au-rich massive sulphide deposits such as the seabed chimneys of the eastern Manus basin[9,30]. □

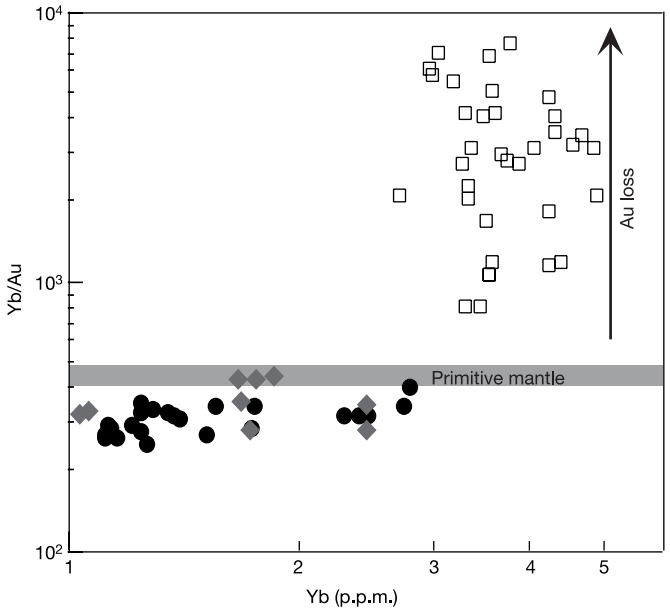

Figure 2 Plot of Yb/Au against Yb showing the relative incompatibility of Au with Yb. The fairly constant Yb/Au for mafic samples (circles) and melt inclusions (diamonds) suggests that Au is moderately incompatible, similarly to Yb. The high and varied Yb/Au of felsic samples (squares) indicates significant Au loss.

Received 16 May; accepted 25 August 2004; doi:10.1038/nature02972.

1. Richards, J. P. Petrology and geochemistry of alkaline intrusives at the Porgera gold deposit, Papua New Guinea. *J. Geochem. Explor.* **35,** 141–199 (1990).
2. Mueller, D. & Groves, D. I. Direct and indirect associations between potassic igneous rocks, shoshonites and gold–copper deposits. *Ore Geol. Rev.* **8,** 383–406 (1993).
3. Sillitoe, R. H. Characteristics and controls of the largest porphyry Cu–Au and epithermal Au deposits in the circum-Pacific region. *Aust. J. Earth Sci.* **44,** 373–388 (1997).
4. Ulrich, T., Guether, D. & Heinrich, C. A. Gold concentrations of magmatic brines and the metal budget of porphyry copper deposits. *Nature* **399,** 676–679 (1999).
5. Mueller, D., Franz, L., Herzig, P. M. & Hunt, S. Potassic igneous rocks from the vicinity of epithermal gold mineralization, Lihir Island, Papua New Guinea. *Lithos* **57,** 163–186 (2001).
6. Mungall, J. E. Roasting the mantle: Slab melting and the genesis of major Au and Au-rich Cu deposits. *Geology* **30,** 915–918 (2002).
7. McInnes, B. I. A., McBride, J. S., Evans, N. J., Lambert, D. D. & Andrew, A. S. Osmium isotope constraints on ore metal recycling in subduction zones. *Science* **286,** 512–516 (1999).
8. Binns, R. A. & Scott, S. D. Actively forming polymetallic sulfide deposits associated with felsic volcanic rocks in the eastern Manus back-arc basin, Papua New Guinea. *Econ. Geol.* **88,** 2226–2236 (1993).
9. Shipboard Scientific Party. Leg 193 Summary. In *Proceedings of the Ocean Drilling Program, Initial Reports* (eds Binns, R. A., Barriga, F. J. A. S. & Miller, D. J.) 1–84 (Ocean Drilling Program, 2002).
10. Togashi, S. & Terashima, S. The behavior of gold in unaltered arc tholeiitic rocks from Izu-Oshima, Fuji, and Osoreyama volcanic areas, Japan. *Geochim. Cosmochim. Acta* **61,** 543–554 (1997).
11. Keays, R. R. & Scott, R. B. Precious metals in ocean-ridge basalts; implications for basalts as source rocks for gold mineralization. *Econ. Geol.* **71,** 705–720 (1976).
12. Zentilli, M., Brooks, R. R., Helgason, J., Ryan, D. E. & Zhang, H. The distribution of Au in volcanic rocks of eastern Iceland. *Chem. Geol.* **48,** 17–28 (1985).
13. Moss, R., Scott, S. D. & Binns, R. A. Gold content of eastern Manus Basin volcanic rocks; implications for enrichment in associated hydrothermal precipitates. *Econ. Geol.* **96,** 91–107 (2001).
14. Williams-Jones, A. E., Migdisov, A. A., Archibald, S. M. & Xiao, Z. Vapor-transport of ore metals. In *Water-Rock Interaction, Ore Deposits, and Environmental Geochemistry: A Tribute to David A. Crerar* (eds Hellman, R. & Wood, S. A.) 279–305 (Spec. Publ. Vol. 7, Geochem. Soc., St Louis, 2002).
15. Loucks, R. R. & Mavrogenes, J. A. Gold solubility in supercritical hydrothermal brines measured in synthetic fluid inclusions. *Science* **284,** 2159–2163 (1999).
16. Sun, W., Bennett, V. C., Eggins, S. M., Arculus, R. J. & Perfit, M. R. Rhenium systematics in submarine MORB and back-arc basin glasses: Laser ablation ICP-MS results. *Chem. Geol.* **196,** 259–281 (2003).
17. Sun, W. D., Bennett, V. C., Eggins, S. M., Kamenetsky, V. S. & Arculus, R. J. Enhanced mantle-to-crust rhenium transfer in undegassed arc magmas. *Nature* **422,** 294–297 (2003).
18. Sun, W. D., Arculus, R. J., Bennett, V. C., Eggins, S. M. & Binns, R. A. Evidence for rhenium enrichment in the mantle wedge from submarine arc volcanic glasses (Papua New Guinea). *Geology* **31,** 845–848 (2003).
19. Kamenetsky, V. S. *et al.* Parental basaltic melts and fluids in eastern Manus backarc basin; implications for hydrothermal mineralisation. *Earth Planet. Sci. Lett.* **184,** 685–702 (2001).
20. Kamenetsky, V. S. *et al.* Fluid bubbles in melt inclusions and pillow-rim glasses: high-temperature precursors to hydrothermal fluids? *Chem. Geol.* **183,** 349–364 (2002).
21. McDonough, W. F. & Sun, S. S. The composition of the Earth. *Chem. Geol.* **120,** 223–253 (1995).
22. Yang, K. & Scott, D. S. Possible contribution of a metal-rich magmatic fluid to a sea-floor hydrothermal system. *Nature* **383,** 420–423 (1996).
23. Yang, K. H. & Scott, S. D. Magmatic degassing of volatiles and ore metals into a hydrothermal system on the modern sea floor of the eastern Manus basin, western Pacific. *Econ. Geol.* **97,** 1079–1100 (2002).
24. Gibert, F., Pascal, M. L. & Pichavant, M. Gold solubility and speciation in hydrothermal solutions: Experimental study of the stability of hydrosulphide complex of gold ($AuHS^0$) at 350 to 450°C and 500 bars. *Geochim. Cosmochim. Acta* **62,** 2931–2947 (1998).
25. Gammons, C. H. & Williams-Jones, A. E. Chemical mobility of gold in the porphyry-epithermal environment. *Econ. Geol.* **92,** 45–59 (1997).
26. Archibald, S. M., Migdisov, A. A. & Williams-Jones, A. E. The stability of Au-chloride complexes in water vapor at elevated temperatures and pressures. *Geochim. Cosmochim. Acta* **65,** 4413–4423 (2001).
27. Phillips, G. N. & Evans, K. A. Role of CO_2 in the formation of gold deposits. *Nature* **429,** 860–863 (2004).
28. Kilinc, A., Carmichael, I. S. E., Rivers, M. L. & Sack, R. O. The ferric-ferrous ratio of natural silicate liquids equilibrated in air. *Contrib. Mineral. Petrol.* **83,** 136–140 (1983).

©2004 Nature Publishing Group

29. Carmichael, I. S. E. & Ghiorso, M. S. Oxidation–reduction relations in basic magma: a case for homogeneous equilibria. *Earth Planet. Sci. Lett.* **78,** 200–210 (1986).
30. Roberts, S. *et al.* Contrasting evolution of hydrothermal fluids in the PACMANUS system, Manus Basin: the Sr and S isotope evidence. *Geology* **31,** 805–808 (2003).

Supplementary Information accompanies the paper on **www.nature.com/nature**.

Acknowledgements We thank S. M. Eggins, C. Allen and J. M. G. Shelley for technical support with the laser-ablation ICP-MS analyses; S.-S. Sun, A. W. Hofmann, J. E. Snow and S. J. Galer for discussions; and A. E. Williams-Jones for a review. This work was supported by a Alexander von Humboldt Research Fellowship to W.D.S. and by a Friedrich Wilhelm Bessel Award to V.S.K. R.J.A. was supported by the Australian Research Council, and R.A.B. by CSIRO and a mineral company consortium.

Competing interests statement The authors declare that they have no competing financial interests.

Correspondence and requests for materials should be addressed to R.J.A. (richard.arculus@anu.edu.au).

A Silurian sea spider

Derek J. Siveter[1,2], Mark D. Sutton[1], Derek E. G. Briggs[3] & David J. Siveter[4]

[1]*Department of Earth Sciences, University of Oxford, South Parks Road, Oxford OX1 3PS, UK*
[2]*Geological Collections, University Museum of Natural History, Oxford OX1 3PW, UK*
[3]*Department of Geology & Geophysics, Yale University, PO Box 208109, New Haven, Connecticut 06520-8109, USA*
[4]*Department of Geology, University of Leicester, Leicester LE1 7RH, UK*

Pycnogonids (sea spiders) are marine arthropods numbering some 1,160 extant species. They are globally distributed in depths of up to 6,000 metres, and locally abundant[1,2]; however, their typically delicate form and non-biomineralized cuticle has resulted in an extremely sparse fossil record that is not accepted universally[3]. There are two opposing views of their phylogenetic position: either within Chelicerata as sister group to the euchelicerates[4–7], or as a sister taxon to all other euarthropods[8]. The Silurian Herefordshire Konservat-Lagerstätte[9] in England (~425 million years (Myr) BP) yields exceptionally preserved three-dimensional fossils that provide unrivalled insights into the palaeobiology of a variety of invertebrates[10–14]. The fossils are preserved as calcitic void in-fills in carbonate concretions within a volcaniclastic horizon[15], and are reconstructed digitally[12]. Here we describe a new pycnogonid from this deposit, which is the oldest adult sea spider by ~35 Myr and the most completely known fossil species. The large chelate first appendage is consistent with a chelicerate affinity for the pycnogonids. Cladistic analyses place the new species near the base of the pycnogonid crown group, implying that the latter had arisen by the Silurian period.

Phylum Arthropoda
Subphylum Chelicerata
Class Pycnogonida
Haliestes dasos gen. et sp. nov.

Etymology. Greek: *Halios* (of the sea) plus *chrestes* (soothsayer; alluding to the forward-facing eye tubercle); *dasys* (hairy) plus *gloutos* (rump).

Holotype. Oxford University Museum of Natural History (OUM) C.29571. Figure 1a–j, reconstructed in three dimensions. The specimen, despite its relatively small size, is interpreted to be an adult on the basis of its completely developed appendages[5], and its long, distally setiferous ovigers probably indicate that it is male[1]. No other material is known.

Horizon and locality. Wenlock Series, Silurian period; Herefordshire, England.

Diagnosis. Pycnogonid with well-developed chelate chelicera, palp and oviger, the last two of which are subchelate; eye tubercle on anterior face of cephalosoma; walking legs subchelate and laterally flattened in the last few segments; rings or annular markings lacking on lateral processes, walking legs and trunk end (referred to as 'abdomen' in traditional pycnogonid terminology).

Description. The combined length of body and trunk end[5] (anterior of cephalosoma to posterior of trunk end) is 3.5 mm. The cephalosoma is sub-pentagonal and slightly swollen where the chelicera, palp and oviger attach, and bears a low eye tubercle on its anterior face (eyes are not preserved). The lateral process is short and narrow. The chelicera (Fig. 1a–e, h) is large and robust and about 0.9 times the body length when extended. The scape consists of two segments, and is similar in length to the chela. The third segment comprises a stout palm and tapering fixed finger, and is opposed by the fourth segment, a movable finger. The fingers overlap slightly in the closed position. (This four-segmented structure contrasts with the three-segmented chelicera of most extant pycnogonids[6].)

The palp (Fig. 1a–e, g) is of similar length to the body. It includes at least eight segments (Fig. 1g). The first and second are the longest, but some segment boundaries are difficult to discern; those identified as segments 2 and 3 may be divided into two. The terminal segments form a subchela. The oviger (Fig. 1a–f), which originates ventro-laterally, is similar in form and length to the palp and comprises nine segments, the first being the longest. Straight, mostly inwardly directed setae occur distally on palp and oviger.

The proboscis (Fig. 1a–e, i) descends very steeply and slightly forwards, and is slightly shorter than the body length. It is sub-circular in cross-section, narrowest about mid-length, and terminates in a small, medial mouth. The pharyngeal lumen shows the characteristic Y-shaped transverse section[16], reflecting the three longitudinal antimeres (Fig. 1c; see also Supplementary Movie). Such a section has not previously been documented in a fossil.

The first walking leg (Fig. 1a–d), comprising nine segments, is at least twice as long as the body. The leg is sub-circular in cross-section proximally, becoming more flattened in the last few segments, and terminating in a subchela. Interpretation of proximal segmentation is based partially on functional considerations (see Supplementary Note 1). The second segment is the longest whereas the seventh is shortest. The third to seventh segments bear pairs of straight, inwardly directed setae, and the eighth a single inward seta. The sixth to eighth segments also bear pairs of outwardly directed setae. The other walking legs (Fig. 1a–d) are similar to the first, but are slightly longer where completely preserved. The first segment of the fourth leg, at least, bears a pair of dorsal setae distally, and probably also proximally. Cement glands and gonopores have not been identified.

The trunk between the cephalosoma and trunk end (Fig. 1a–d) is about 0.7 times the body length. Two small, axial, forwardly directed setae or spines occur anterior to the third walking leg; similar processes are indicated weakly elsewhere on the trunk. The second to fourth lateral processes are better differentiated than the first and are directed increasingly more posteriorly, particularly the fourth.

The trunk end (Fig. 1a, b, d, j) is about 0.18 times the body length. In lateral view it comprises three 'elements' (segment boundaries have not been discerned); the proximal and distal elements are shorter and inclined slightly upwards and downwards respectively, whereas the central element is near horizontal. The central section bears an axial node posteriorly, with two pairs of setae: one pair directed postero-dorsally, the other postero-ventrally (Fig. 1j). Between this node and the trunk there is a suggestion of one or possibly two short, axial setae or spine bases. The position of the anus is unknown.

©2004 Nature Publishing Group

Release of gold-bearing fluids in convergent margin magmas prompted by magnetite crystallization

Weidong Sun*†, Richard J. Arculus†, Vadim S. Kamenetsky*‡, Raymond A. Binns†✳

** Max-Planck Institut f. Chemie, Mainz, Postfach 3060, Mainz, 55020, Germany*
† Research School of Earth Sciences, Australian National University, Canberra, ACT 0200, Australia
† Department of Earth and Marine Sciences, Australian National University, Canberra, ACT 0200, Australia
‡ Centre for Ore Deposit Research and School of Earth Sciences, University of Tasmania, GPO Box 252-79, Hobart, Tasmania, 7001, Australia
✳ CSIRO Exploration and Mining, North Ryde, NSW 1670, Australia

Supplementary Information

Geological setting of Manus Basin and sample description

The Manus Basin in the southwestern Pacific is an actively spreading back-arc basin surrounded by the islands of New Britain, New Ireland, New Guinea and Manus, bounded to the north by the now inactive Vitiaz trench and to the south by New Britain trench and associated arc[1,2]. Tectonically, it is part of the Pacific/Bismarck plate boundary where plate motion takes place along three major left-lateral transform faults and a range of different extensional segments[3]. The rock types in the whole Manus Basin range from normal MORB to arc-like compositions[4,5]. The eastern Manus Basin is characterized by the arc type magmas. This region has been above subduction zones for more than 40 Ma[6,7]. The studied set of submarine (1640 - 2000 m water depth) quenched glasses from the eastern Manus Basin represents a fractionating series (see Figure 1), ranging from basalt and basaltic andesite to dacite and rhyodacite. These glasses possess a strong subduction-related geochemical signature (e.g., Nb, Ta depletion, and Cs, Rb, Ba, Pb enrichment, which are typical for arc magmas)[8].

Supplementary Table 1. Sample location and description

Dredge	CSIRO Sample #	Latitude S	Longitude E	Depth m
MD-6	107162	3º 42.0'	151º 46.0'	1780
MD-39	118497	3º 40.5'	151º 44.8'	1785
87-DR	118866	3º 36.6'	151º 47.3'	1900
MD-28	118349, *	3º 43.6'	151º 40.3'	1680
MD-65	132496	3º 43.7'	151º 40.1'	1715
MD-114	134306	3º 43.8'	151º 40.0'	1665
MD-36	118483, *	3º 42.8'	151º 42.7'	1850
MD-53	132253	3º 42.6'	151º 41.3'	1680
MD-7	107243	3º 40.4'	151º 44.5'	1840
86-DR	118856	3º 36.7'	151º 49.5'	2000
MD-101	134043	3º 41.0'	151º 33.3'	1640
MD-3	107094	3º 42.8'	151º 36.8'	1950
MD-38	*	3º 35.8'	151º 40.8'	2000

*reference 6

Analytical methods

Gold was determined using a laser ablation inductively coupled plasma mass spectrometry (LA-ICP-MS) method refined for analyzing ppb to sub-ppb levels of trace elements[9-11], which is particular useful for analyzing small samples like olivine hosted melt inclusions and glass pieces.

Gold has only one isotope (^{197}Au) and therefore the laser results cannot be calibrated using isotope dilution method as done for Re[9].

The potential ^{181}Ta^{16}O interference was corrected as follows: TaO/Ta was determined using both Ta metal and TaO powder; Ta metal gives fairly constant TaO/Ta of 0.00025 to 0.00028; the TaO powder gives TaO/Ta of 0.00034 to 0.00044. The real TaO/Ta value of samples and standard glasses should be somewhere in between. In this study, the ^{181}Ta^{16}O interference was corrected using the highest TaO/Ta (0.00044), which may introduce systematic errors. Nevertheless, the difference between corrected and uncorrected results ranges from –1% to 10%, within the analytical errors.

Using a reference value of 4.58 ppm for Au in NIST 612, a concentration of 21.8±0.2 ppm was obtained for NIST 610, which is identical within error to the solution ICP-MS result of 22.1 ppm[12]. That for NIST 617 is 0.215±0.004 ppm, about 10% higher than the solution ICP-MS result (0.197 ppm)[12]. Similarly, systematic offset of about 10% has been reported for LA-ICP-MS results for ppb to sub-ppb levels of Re, suggesting that this offset is probably related to the extreme working conditions of the LA-ICP-MS adopted in this study. Considering that we do not have a better method to calibrate the LA-ICP-MS results, and that 10% is within the statistical errors, the offset has not been corrected.

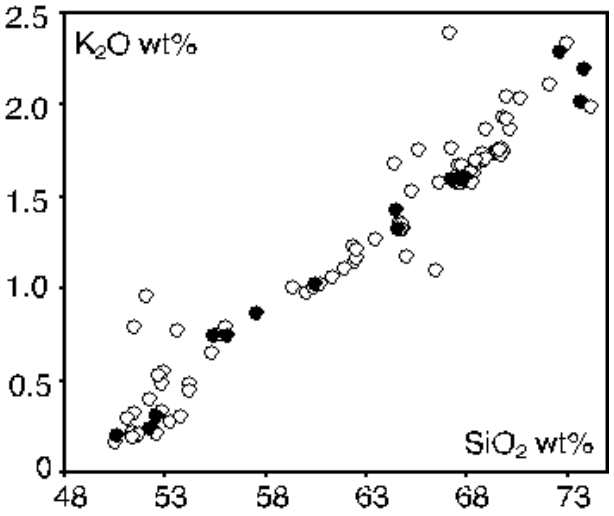

Supplementary Figure 1. **SiO_2 versus K2O.**

The eastern Manus Basin suite studied here was selected from a larger group recovered from the Eastern Rifts in the Basin, with coherent major and trace element fractionation patterns consistent with co-genetic relationships dominated by fractional crystallisation of a common parent magma type (Data: filled circles, samples studied in this contribution; open circles, CSIRO conventional bulk rock analyses).

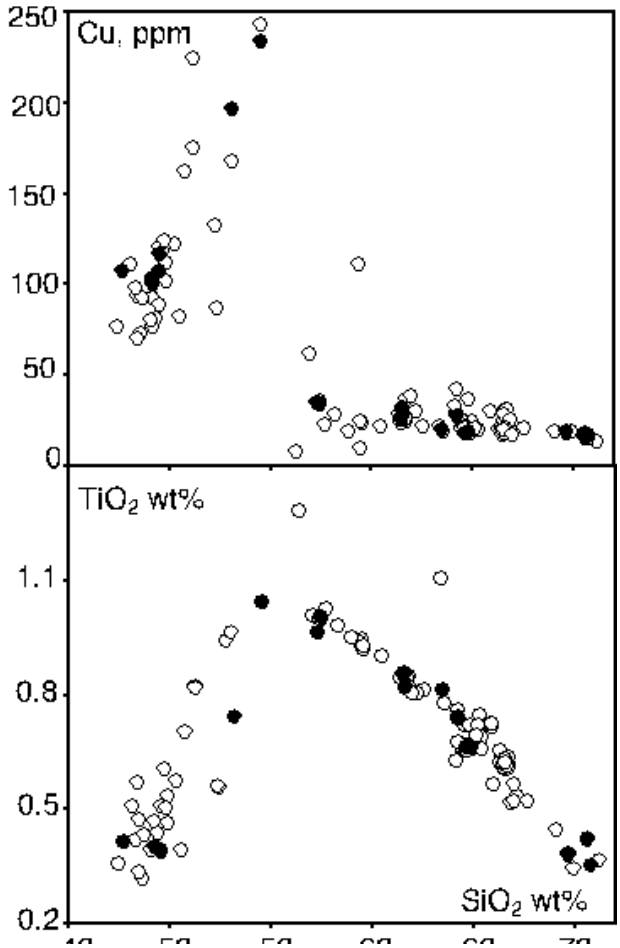

Supplementary Figure 2. **SiO_2 versus TiO_2 and Cu.**

The behaviour of TiO_2 changes at ~ 58wt% SiO_2 contents, which marks the commencement of titanomagnetitie crystallization. The concentration of Cu changes sharply at the same point, indicating sharp Cu loss when magnetite starts to crystallize (symbols are the same as Figure 1).

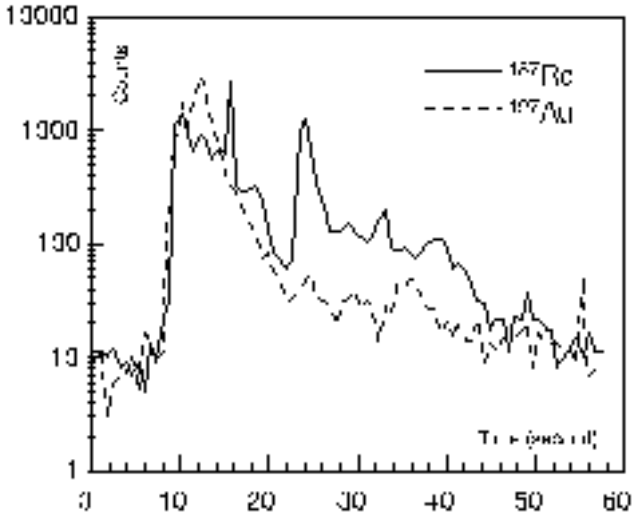

Supplementary Figure 3. **Signal spectra of Re and Au for a piece of glass of a heterogeneous sample (87DR-II).**

For most of the samples, Au signals are ~10 times higher than the background (~0.8 counts). For the heterogeneous sample, both Re and Au are remarkably higher than other samples, the peaks of Re and Au, however, are not coherent, indicating that Au and Re are hosted by different minerals (e.g., sulphides in fluid bubbles[6]).

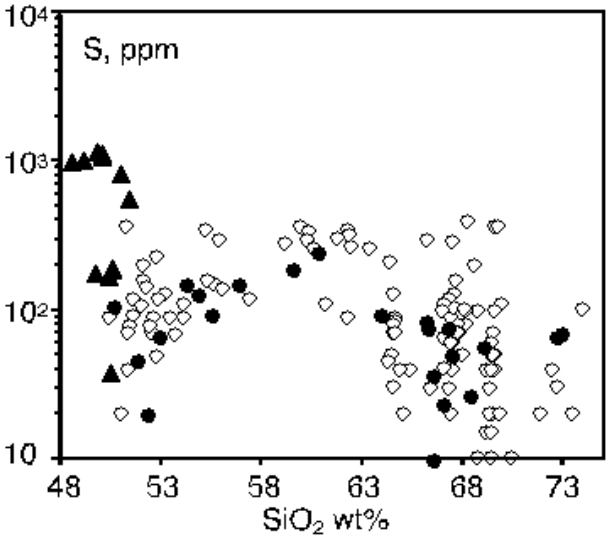

Supplementary Figure 4. **Sulfur versus SiO_2.**

Sulphur abundances in melt inclusions, although varied, are much higher than in glasses at a given SiO_2 content,

of S have been lost, most likely through degassing. This S loss however, did not significantly affect the chalcophile element abundances in the mafic magmas. The most likely reason is that S was lost mainly in the form of sulphate. This hypothesis is supported by the fact that sulphate species dominate over sulphide species in olivine-hosted fluid bubbles[6,14], due to high fO_2. Filled triangles represent melt inclusions; other symbols as in Figure 1.

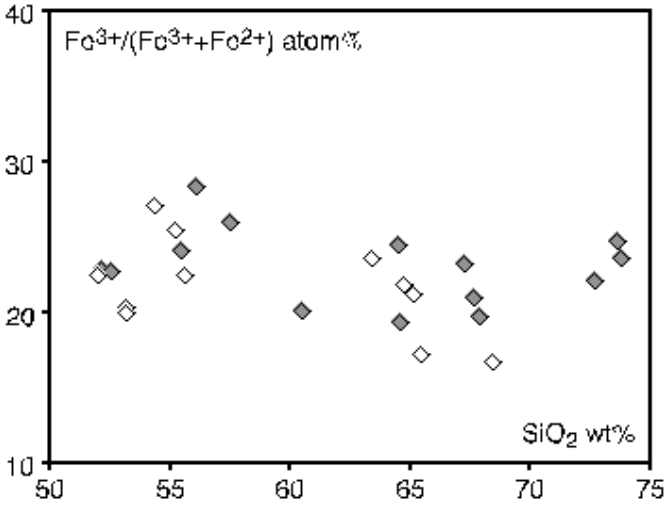

Supplementary Figure 5. **$Fe^{3+}/(Fe^{3+} + Fe^{2+})$ x 100 versus SiO_2**

The $Fe^{3+}/(Fe^{3+} + Fe^{2+})$ is fairly constant (~23 atom%) through the whole range of magma fractionation, which corresponds to 2 $\log_{10}$orders more oxidized than the synthetic fayalite-magnetite-quartz buffer. This indicates redox buffering during magma fractionation. Grey diamonds are from this study; open diamonds from[4].

---

1. Moss, R., Scott, S. D. & Binns, R. A. Gold content of eastern Manus Basin volcanic rocks; implications for enrichment in associated hydrothermal precipitates. *Economic Geology* **96**, 91-107 (2001).
2. Taylor, B. *Backarc Basins: Tectonics and magmatism* (Plenum, NY, 1995).
3. Martinez, F. & Taylor, B. Backarc spreading, rifting, and microplate rotation, between transform faults in the Manus Basin. *Marine Geophysical Researches* **18**, 203-224 (1996).
4. Sinton, J. M., Ford, L. L., Chappell, B. W. & McCulloch, M. T. Magma genesis and mantle heterogeneity in the Manus back-arc basin, Papua New Guinea. *Journal of Petrology* **44**, 159-195 (2003).
5. Taylor, B. & Martinez, F. Back-arc basin basalt systematics. *Earth and Planetary*
6. Kamenetsky, V. S. et al. Parental basaltic melts and fluids in eastern Manus backarc basin; implications for hydrothermal mineralisation. *Earth and Planetary Science Letters* **184**, 685-702 (2001).
7. Exon, N. F., Stewart, W. D., Sandy, M. J. & Tiffin, D. L. Geology and offshore petroleum prospects of the eastern New Ireland Basin, northeastern Papua New Guinea. *BMR J. Aust. Geol. Geophys.* **10**, 39-51 (1986).
8. McCulloch, M. T. & Gamble, A. J. Geochemical and geodynamical constraints on subduction zone magmatism. *Earth and Planetary Science Letters* **102**, 358-374 (1991).
9. Sun, W., Bennett, V. C., Eggins, S. M., Arculus, R. J. & Perfit, M. R. Rhenium systematics in submarine MORB and Back-arc basin glasses: Laser ablation ICP-MS results. *Chemical Geology* **196**, 259-281 (2003).
10. Sun, W. D., Bennett, V. C., Eggins, S. M., Kamenetsky, V. S. & Arculus, R. J. Enhanced mantle-to-crust rhenium transfer in undegassed arc magmas. *Nature* **422**, 294-297 (2003).
11. Sun, W. D., Arculus, R. J., Bennett, V. C., Eggins, S. M. & Binns, R. A. Evidence for rhenium enrichment in the mantle wedge from submarine arc volcanic glasses (Papua New Guinea). *Geology* **31**, 845-848 (2003).
12. Sylvester, P. J. & Eggins, S. M. Analysis of Re, Au, Pd, Pt and Rh in NIST glass certified reference materials and natural basalt glasses by laser ablation ICP-MS. *Geostandards Newsletter* **21**, 215-229 (1997).